ADVANCED MATERIALS
www.advmat.de

Rational Ligand Design of Conjugated Coordination Polymers for Efficient and Selective Nitrate Electroreduction to Ammonia

Shouhan Zhang, Yan Liu, Yidan Ding, Hangjuan Wu, Li Qing, Jiexin Zhu, Shenghua Chen, Ziyun Wang, Longsheng Zhang,* and Tianxi Liu**

Electrocatalytic nitrate reduction to ammonia (NRA) offers an attractive route for converting nitrate pollutants to ammonia under mild conditions. Among other catalysts, single-atom catalysts (SACs) with high metal-atom-utilization efficiency and low-coordinated metal sites hold immense potential to be extensively applied, which unfortunately encounter a formidable challenge to obtain simultaneous improvement of NRA activity and selectivity. Here, a novel and general strategy is reported to achieve efficient and selective NRA catalysis on conjugated coordination polymers featuring with high-density and well-defined nitrogen (N)-coordinated single-atom metal sites via precise regulation of N-heterocyclic ligands toward accelerating the hydrogenation kinetics necessitated in the NRA pathway. Taking cobalt (Co) as an example, two CoN_4-centered conjugated coordination polymer electrocatalysts (CoN_4-pyrr and CoN_4-pyri) are synthesized with pyrrole and pyridine ligands are investigated as a proof-of-concept study. As revealed, the CoN_4-pyrr can markedly outperform the CoN_4-pyri toward NRA electrocatalysis. Experimental and theoretical results suggest that, relative to the N atoms of pyridine ligand in CoN_4-pyri, the N atoms of pyrrole ligand in CoN_4-pyrr can enable a faster transfer of hydrogen radicals to the Co active sites for accelerating the hydrogenation kinetics of $^*NO$ intermediate at the rate-determining step of NRA pathway.

1. Introduction

Ammonia (NH_3) serves as a crucial feedstock for both industrial and agricultural sectors and stands out as a hydrogen storage carrier with high hydrogen content.[1,2] However, the Haber–Bosch method renders harsh reaction requirements (≈500 °C and ≈300 atm), large energy consumption and carbon emission.[3] Electrocatalytic nitrogen reduction reaction has profoundly emerged as a promising alternative for efficient NH_3 synthesis at mild conditions.[4] Nevertheless, the nitrogen reduction reaction process is hindered by the high N≡N bond energy of N_2 and the intense competition from the hydrogen evolution reaction (HER), limiting the enhancement of the N_2 fixation efficiency.[5–7] In contrast, electrocatalytic nitrate reduction to ammonia (NRA) renders comparatively faster reaction rates owning to the lower N═O bond energy of NO_3^-.[8] Moreover, NRA electrocatalysis can efficiently promote the conversion of widespread NO_3^- pollutants into NH_3, representing a promising approach for NH_3 electrosynthesis and wastewater treatment under mild conditions.[9] Furthermore, the NH_3 products generated in the NRA process can be separated by many methods such as air stripping technology and hydrophobic membrane permeation.[10,11]

A wide range of electrocatalysts have been developed including metal, metal alloy, metal compound, carbonaceous material, single-atom catalyst (SAC) and etc.[12–18] Among others, SACs have particularly attracted tremendous attentions owing to their maximum metal-utilization efficiency and low-coordinated

S. Zhang, Y. Ding, L. Qing, L. Zhang, T. Liu
Key Laboratory of Synthetic and Biological Colloids
Ministry of Education
School of Chemical and Material Engineering
Jiangnan University
Wuxi 214122, P. R. China
E-mail: zhangls@jiangnan.edu.cn; txliu@jiangnan.edu.cn

Y. Liu, Z. Wang
School of Chemical Sciences
University of Auckland
Auckland 1010, New Zealand
E-mail: ziyun.wang@auckland.ac.nz

H. Wu, S. Chen
National Innovation Platform (Center) for Industry-Education Integration of Energy Storage Technology
Xi'an Jiaotong University
Xi'an, Shanxi 710049, P. R. China

J. Zhu
Department of Mechanical and Industrial Engineering
University of Toronto
Toronto, ON M5S 3G8, Canada

The ORCID identification number(s) for the author(s) of this article can be found under https://doi.org/10.1002/adma.202418681

DOI: 10.1002/adma.202418681

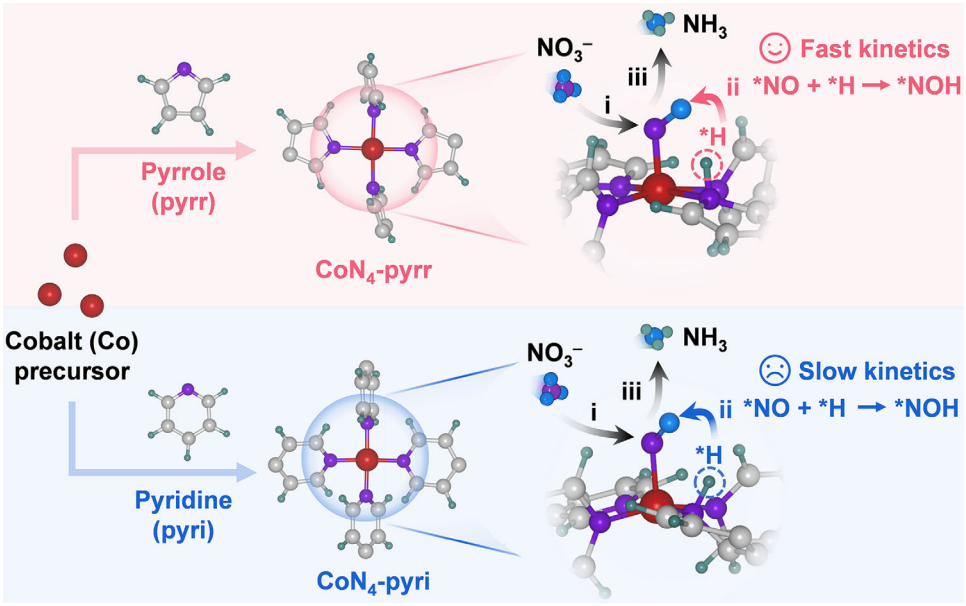

Figure 1. Schematic illustration of the molecular structures of CoN_4-pyrr and CoN_4-pyri catalysts with well-defined single-atom Co sites with CoN_4 coordination structures as well as the proposed NRA mechanism: i) adsorption/conversion of NO_3^- into $^*NO$, ii) hydrogenation of $^*NO$ into $^*NOH$ at the rate-determining step, and iii) conversion of $^*NOH$ into $^*NH_3$ and desorption of NH_3. Relative to the N atom of the pyridine ligand in CoN_4-pyri, the N atom of the pyrrole ligand in CoN_4-pyrr can enable a faster transfer of $^*H$ for accelerating the hydrogenation kinetics of $^*NO$ intermediate on the Co active site at the rate-determining step toward NRA electrocatalysis.

metal sites.[19–22] Despite the significant progress that have been achieved, previous design strategies of SACs often render uncontrollable and inflexible regulation of the coordination structures of metal centers in the SACs, especially those prepared via high-temperature calcination approaches.[23–28] A strong adsorption of NRA intermediates on the metal centers of SACs would result in enhanced NRA selectivity yet decreased NRA activity arising from the suppressed desorption of NRA intermediates, while a weak adsorption of NRA intermediates would allow excessive adsorption of HER intermediates and exacerbate the competitive HER. Along the NRA pathway, the hydrogenation process of NO_3^- to produce NH_3 is necessitated, which critically depends on the hydrogen ($^*H$) radicals generated near the metal centers of SACs.[29–33] Sluggish water dissociation kinetics in alkaline media would hinder the competitive HER for enhancing the NRA selectivity, and on the other hand, lead to insufficient $^*H$ supply to accelerate the hydrogenation kinetics for enhancing the NRA activity.[34,35] It is desired yet remains challenging to tailor the $^*H$ supply near the single-atom metal sites of SACs to obtain simultaneous improvement of NRA activity and selectivity.

Here, we report a facile and general strategy to enhance the hydrogenation kinetics of SACs toward boosting their NRA activity and selectivity through precisely tailoring the nitrogen-heterocyclic ligands of conjugated coordination polymer electrocatalysts, which as a paradigm of SACs feature high-density single-atom metal sites with well-defined coordination structures. By readily modulating the functional groups of ligands, the coordination structures of the single-atom metal sites within conjugated coordination polymers can be controllably regulated.[36,37] As shown in **Figure 1**, for the proof-of-concept studies, two analogous cobalt (Co)-single-atom based conjugated coordination polymer catalysts synthesized with pyrrole and pyridine ligands (denoted as CoN_4-pyrr and CoN_4-pyri, respectively) were investigated. Notably, pyrrole consists of a pentagonal ring with the lone pair electrons of its N atoms featuring profound π-delocalization within its conjugated structures. By comparison, pyridine consists of a hexagonal ring with the lone pair electrons of its N atoms not participating in the π-delocalization in its conjugated structures. Despite previous studies about the molecular catalysts prepared with pyridine or pyrrole ligands, systematic investigation is lacked for the influence of the N atoms of pyrrole and pyridine ligands on the hydrogenation kinetics on the Co active sites adjacent to the N atoms within CoN_4-pyrr and CoN_4-pyri. Our electrochemical results indicate that the CoN_4-pyrr catalyst exhibits markedly higher NRA activity and selectivity with superior NH_3 yield rate (1.93 mmol h^{-1} cm^{-2}) and NH_3 Faradaic efficiency (99.5%) at a current density of 380.3 mA cm^{-2}, surpassing the CoN_4-pyri catalyst and other SACs toward NRA electrocatalysis. Further, theoretical calculations unravel that, relative to the N atoms of pyridine ligand in the CoN_4-pyri catalyst, the $^*H$ adsorbed at the N atoms of pyrrole ligand in the CoN_4-pyrr catalyst can enable a faster kinetics of $^*H$ transfer and subsequent $^*NO$ hydrogenation over Co active sites at the rate-determining step along NRA pathway. The required energy barrier for CoN_4-pyrr is appreciably lower than that for CoN_4-pyri, accounting for its improved NRA performance as observed in experiment. More significantly, considering the exceptional adjustability of single-atom metal sites in the conjugated coordination polymers arising from the diversities of ligands and metal precursors, such strategy can be prospectively applied to prepare high-performance SACs targeted toward various catalytic reactions.

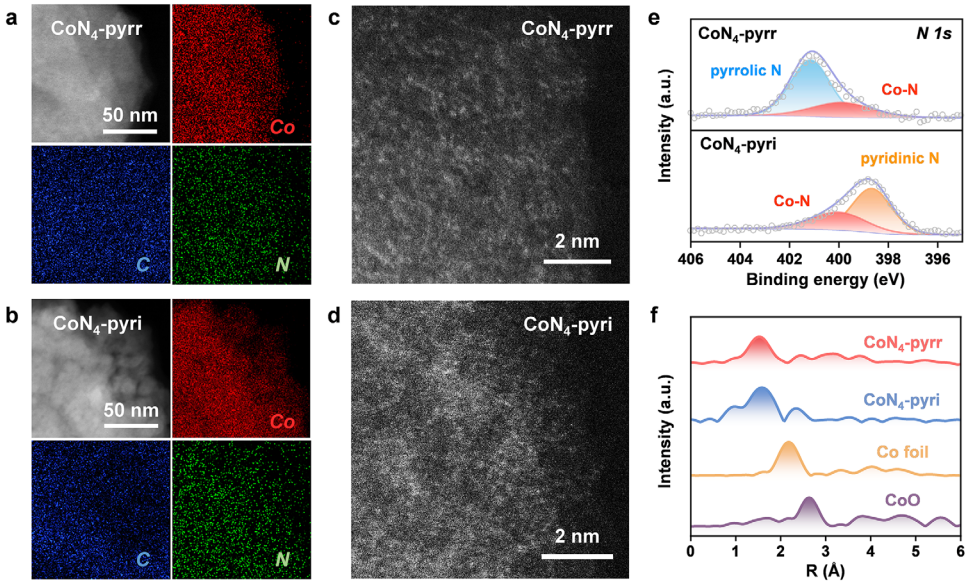

Figure 2. a,b) TEM and the elemental mapping images of CoN_4-pyrr and CoN_4-pyri, respectively. c,d) HAADF-STEM images of CoN_4-pyrr and CoN_4-pyri, respectively. e,f) N 1s XPS spectra and EXAFS spectra CoN_4-pyrr and CoN_4-pyri, respectively.

2. Results and Discussion

2.1. Morphological and Structural Analysis

We first synthesized the CoN_4-pyrr and CoN_4-pyri catalysts by a facile hydrothermal approach (see details in Experimental Section, Supporting Information). Scanning electron microscopy (SEM) observations present that the CoN_4-pyrr is sheet-like and the CoN_4-pyri is nanoparticle-like (Figure S1, Supporting Information). The transmission electron microscopy (TEM) images and corresponding elemental mapping analysis (**Figure** 2a,b) present the uniform distributions of Co, C, and N elements within the CoN_4-pyrr and CoN_4-pyri catalysts. The high-angle annular dark-field scanning transmission electron microscopy (HAADF-STEM) images of CoN_4-pyrr and CoN_4-pyri both feature many atomically dispersed bright spots that are identified as Co single atoms (Figure 2c,d). As examined by inductively coupled plasma-mass spectrometry analysis, the Co weight percentage in the CoN_4-pyrr and CoN_4-pyri catalysts are 24.7 and 22.4 wt.% (Table S1, Supporting Information), respectively. As seen Figure S2 (Supporting Information), the powder X-ray diffraction patterns of CoN_4-pyrr and CoN_4-pyri present no characteristic peak of metallic Co component. X-ray photoelectron spectroscopy (XPS) tests were carried out to examine the chemical environment and bonding information of the catalysts. As displayed in Figures S3 and S4 (Supporting Information), the binding energies of Co $2p_{3/2}$ and Co $2p_{1/2}$ peaks for CoN_4-pyrr feature a positive shift of 0.2 eV relative to those for CoN_4-pyri, indicating its higher oxidation states of Co sites.[38,39] As shown in the N 1s XPS spectra (Figure 2e), the peaks at 401.2 and 399.9 eV that can be ascribed to the pyrrolic N and Co—N bond for CoN_4-pyrr, while the peaks at 398.6 and 399.9 eV can be ascribed to the pyridinic N and Co—N bond for CoN_4-pyri.[40,41] As shown in Figure S5 (Supporting Information), the Fourier transform infrared (FTIR) spectra of CoN_4-pyrr and CoN_4-pyri both show two characteristic peaks at 1638 and 1385 cm^{-1}, which can be assigned to the C═N stretching vibration and C—N stretching vibration, respectively.[42] Moreover, the CoN_4-pyrr and CoN_4-pyri both show a peak at 833 cm^{-1}, which is related to Co—N bonds.[43] These FTIR results, in conjunction with the N 1s XPS results, can verify the metal-ligand coordination of Co metal with pyrrole and pyridine ligands within the CoN_4-pyrr and CoN_4-pyri.

Furthermore, Co *K*-edge X-ray absorption near-edge structure (XANES) and extended X-ray absorption fine structure (EXAFS) spectroscopy were performed to study the coordination structures of Co sites in CoN_4-pyrr and CoN_4-pyri. As seen in the XANES spectra (Figure S6, Supporting Information), the absorption edge of CoN_4-pyrr is higher than that of CoN_4-pyri, indicating the higher valence of Co sites in the CoN_4-pyrr. Additionally, as shown in Figure 2f, the prominent peaks in the EXAFS spectra at *R* space for CoN_4-pyrr and CoN_4-pyri can be attributed to Co—N coordination, distinctly different from the Co—Co peak of Co foil at 2.1 Å. No Co—Co contribution peaks are found in the EXAFS spectra of CoN_4-pyrr and CoN_4-pyri, verifying the Co-single-atom features in these two catalysts. Note that the peaks observed at 2.5 Å for CoN_4-pyrr and CoN_4-pyri can be attributed to Co—C contribution. The fine *K*-space EXAFS oscillations for these samples suggest the high reliability of EXAFS data. (Figure S7, Supporting Information). Direct comparisons of the wavelet transform contour plots (Figure S8, Supporting Information) can confirm the Co-single-atom characteristics of CoN_4-pyrr and CoN_4-pyri, which both exhibit an intensity maximum attributed to the Co—N coordination, different from those for Co foil and CoO. Besides, the best EXAFS fitting results (Figure S9 and Table S2, Supporting Information) can suggest that the Co—N coordination numbers of Co single atoms within the CoN_4-pyrr and CoN_4-pyri are both ≈4. These results validate the successful synthesis of the CoN_4-pyrr and CoN_4-pyri catalysts featuring abundant single-atom Co sites with well-defined CoN_4 coordination structures.

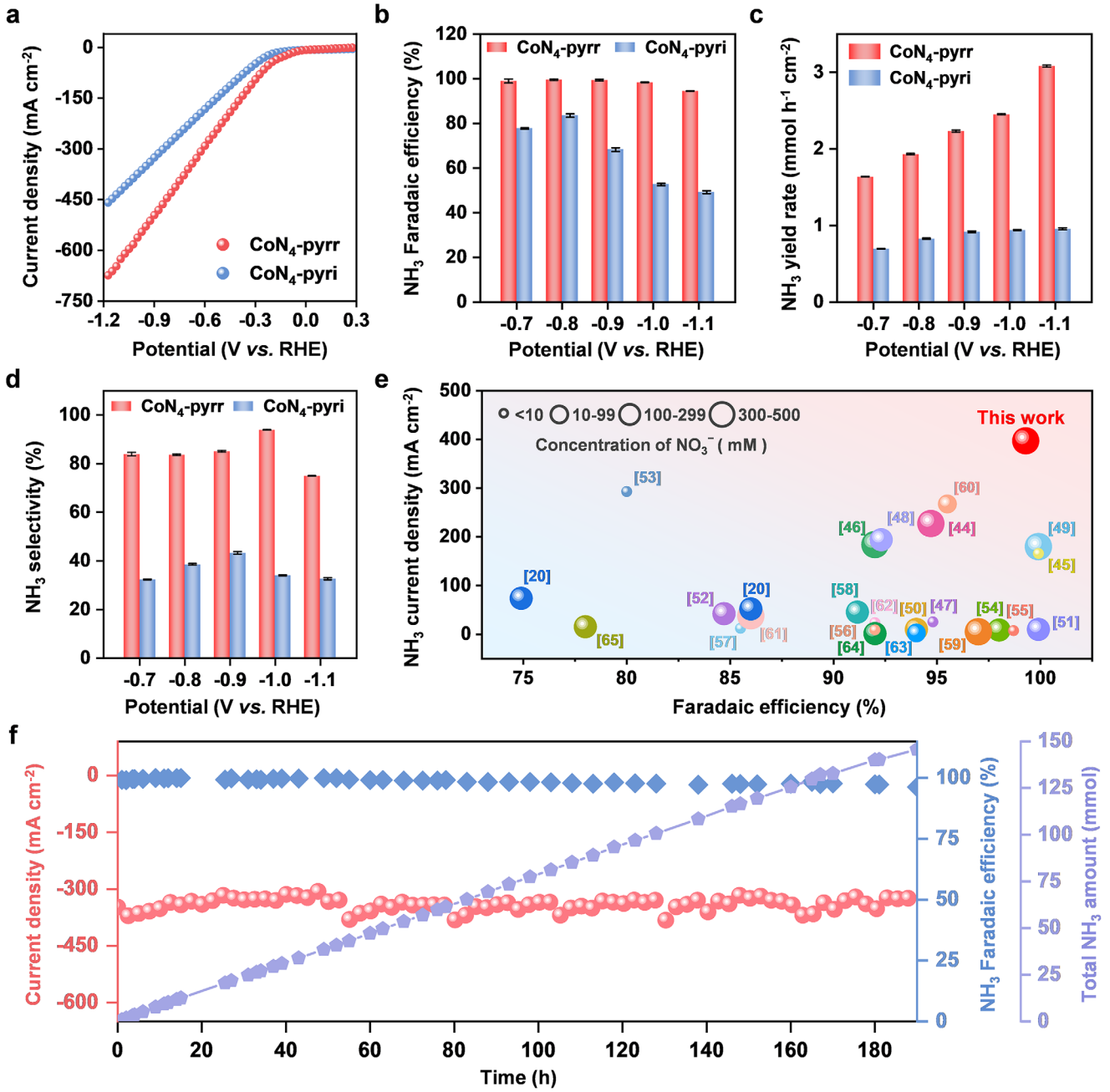

Figure 3. a) LSV curves for CoN_4-pyrr and CoN_4-pyri electrodes measured in 1 M KOH aqueous electrolyte with 500 mM NO_3^-. b–d) Comparisons of NH_3 Faradaic efficiency, NH_3 yield rate, and NH_3 selectivity for CoN_4-pyrr and CoN_4-pyri electrodes, respectively. e) Performance comparison between CoN_4-pyrr and other reported SACs toward NRA electrocatalysis. f) NH_3 Faradaic efficiency and NH_3 yield rate for CoN_4-pyrr during the chronoamperometry test.

2.2. Electrochemical Performance Evaluation

Electrocatalytic NRA performance of CoN_4-pyrr and CoN_4-pyri catalysts were assessed in a H-type electrolysis cell using 1 M KOH aqueous electrolyte with 500 mM NO_3^-. As seen in Table S3 (Supporting Information), the CoN_4-pyrr and CoN_4-pyri catalyst electrodes present similar electrical conductivity. The linear sweep voltammetry (LSV) analysis showed an obvious increase in current density when the NO_3^- were introduced into the electrolyte, validating the occurrence of NO_3^- electroreduction (Figure S10, Supporting Information). Moreover, as exhibited in **Figure** 3a, the CoN_4-pyrr electrode exhibits substantially higher current densities than the CoN_4-pyri electrode, suggesting its superior activity toward NRA electrocatalysis. The Faradaic efficiencies of NH_3 products were quantified through using colorimetric methods with UV–vis spectroscopy measurements (Figure S11, Supporting Information). As seen in Figure 3b,c, the NH_3 Faradaic efficiencies and NH_3 yield rates obtained for the

CoN_4-pyrr electrode are largely higher than those obtained for the CoN_4-pyri electrode under various applied potentials referenced to the reversible hydrogen electrode (RHE). The NH_3 Faradaic efficiency for CoN_4-pyrr electrode reaches 99.5% at −0.8 V (vs RHE) with a superior NH_3 yield rate of 1.93 mmol h^{-1} cm^{-2}, markedly higher than those of CoN_4-pyri. Moreover, the CoN_4-pyrr electrode achieves a maximum NH_3 yield rate of 3.08 mmol h^{-1} cm^{-2} at −1.1 V (vs RHE) while maintaining a NH_3 Faradaic efficiency as high as 94.4%. By normalizing the NH_3 products by the loading mass of catalysts (Figure S12, Supporting Information), the NH_3 yield rates obtained for CoN_4-pyrr electrode are 5.82 and 8.86 mmol h^{-1} mg^{-1} at −0.8 and −1.1 V (vs RHE), respectively. Significantly, as seen in Figure S13 (Supporting Information), with various concentration of NO_3^- (e.g., 50, 100, and 250 mM) in the electrolyte, the NH_3 Faradaic efficiencies and NH_3 yield rates obtained for CoN_4-pyrr electrode are all substantially higher than those for CoN_4-pyri electrode. Moreover, as seen in Figure S14 (Supporting Information), after 7 h of NRA catalysis over the CoN_4-pyrr electrode, 3.19 μg mL^{-1} of NO_3^- remained in the final electrolyte, which falls below the WHO limit for drinking water (NO_3^- < 11.3 μg mL^{-1}).

Further, isotopic labeling experiments were performed by utilizing $^{14}NO_3^-$ and $^{15}NO_3^-$ as the reactants for the NRA electrocatalysis, respectively. As presented in Figure S15 (Supporting Information), the ^1H nuclear magnetic resonance spectroscopy results reveal that the typical triplet peaks of $^{14}NH_4^+$ at δ = 7.00, 7.13, and 7.26 ppm and double peaks of $^{15}NH_4^+$ located at δ = 6.98 and 7.16 ppm can be correspondingly observed for the NRA electrocatalysis proceeded with $^{14}NO_3^-$ and $^{15}NO_3^-$ sources in the electrolytes. Moreover, as presented in Figures S16 and S17 (Supporting Information), negligible NH_3 products were detected from the control electrochemical experiments performed without NO_3^- in the electrolyte, without applied potential and without catalyst, thus verifying that the NH_3 products are originated from the NRA electrocatalysis rather than the interferences from catalyst or electrolyte. Furthermore, we then evaluated the specific activities of CoN_4-pyrr and CoN_4-pyri by determining their NH_3 partial current densities concerning their electrochemical active surface areas (Figures S18–S20, Supporting Information), which reveals the markedly higher specific activity of CoN_4-pyrr catalyst in comparison with CoN_4-pyri catalyst. Additionally, we also investigated the NH_3 selectivity of these two catalysts (Figure 3d; Figure S21, Supporting Information), unveiling that the CoN_4-pyrr electrode exhibits a substantially higher NH_3 selectivity (≈ 80%) than that of CoN_4-pyri electrode (≈ 40%) under various potentials. As seen in Figures S22 and S23 (Supporting Information), the Faraday efficiency of NO_2^- byproduct for CoN_4-pyrr is lower than that of CoN_4-pyri, indicating its superior selectivity. More significantly, as demonstrated in Figure 3e and Table S4 (Supporting Information), the CoN_4-pyrr electrode outperforms other reported SACs toward NRA catalysis.[20,44–65] Furthermore, as exhibited in Figure 3f and Figure S24 (Supporting Information), during the chronoamperometry measurement of the CoN_4-pyrr electrode at −0.8 V (vs RHE) for over 190 h, the fluctuations of NH_3 Faradaic efficiencies are within a reasonable range with a steadily cumulative yield of NH_3 products, showcasing its exceptional durability for NRA electrocatalysis. As seen in (Figure S25, Supporting Information), negligible variation of the pH value before and after the electrochemical test was observed. The XRD, XPS, and EXAFS analysis for CoN_4-pyrr show that a negligible structural change of their single-atom Co active sites is observed before and after NRA electrocatalysis. (Figures S26 and S27, Supporting Information).

2.3. Catalytic Mechanism Investigation

We further conducted in situ FTIR experiments to capture possible intermediates over the CoN_4-pyrr and CoN_4-pyri catalysts (Figure S28, Supporting Information) during the NRA process. The observed peaks located at ≈ 1660 and 1240 cm^{-1} can be attributed to the $^*NO$ and $^*NO_2$ intermediates, respectively.[66,67] As the potential varied from −0.1 to −1.1 V, the peak intensity increasements of $^*NO$ and $^*NO_2$ intermediates for CoN_4-pyrr are more pronounced compared to those of CoN_4-pyri, indicating its faster kinetics of NO_3^- adsorption/reduction, in agreement with those results from the electrochemical performance evaluation. Differential electrochemical mass spectroscopy (DEMS) was further conducted to capture the signal of reaction intermediates of NRA (**Figure 4a**; Figure S29, Supporting Information). The m/z signals of 17, 16, 15, 14, and 31 correspond to the $^*NH_3$, $^*NH_2$, $^*NH$, $^*N$ and $^*NOH$, respectively, appeared during continuous five cycles. Furthermore, under in situ operation, $^*NO$ was hydrogenated to $^*NOH$ by $^*H$, which was deoxygenated to $^*N$. Afterward, $^*N$ was hydrogenated into $^*NH$, $^*NH_2$, and $^*NH_3$ owing to the strong hydrogenating capability of CoN_4-pyrr. As revealed by the DEMS analysis, the pathway of NRA can be deduced and the free energies of reaction intermediates over the CoN_4-pyrr and CoN_4-pyri were calculated (Figure S30, Supporting Information). The Gibbs free energy profiles along the NRA pathway were computed through using density functional theory (DFT) calculations for the CoN_4-pyri and CoN_4-pyrr models well as the benchmark CoNC model. Each reaction step from $^*NO_3$ to $^*NH_3$ are elaborately displayed in the free energy diagrams (Figures S31–S33, Supporting Information). The hydrogenation step from $^*NO$ to $^*NOH$ is determined as the rate-determining step, as identified by the highest energy barrier, marking it as the most energetically demanding transition along the NRA pathway. The computed free energy results (Figure 4b; Figure S34 and Table S5, Supporting Information) revealed that the CoN_4-pyrr model exhibited an activation energy of 0.90 eV, which is significantly lower than those of the CoN_4-pyri model (1.12 eV) and CoNC model (1.34 eV) at the rate-determining step along the NRA pathway, indicating its higher efficiency toward facilitating this critical hydrogenation step.

Moreover, regarding the hydrogenation of $^*NO$ to form $^*NOH$, the adsorption energy of hydrogen for the CoN_4-pyrr model was computed to be 0.22 eV, markedly lower than that (1.21 eV) for the CoN_4-pyri model (Figure 4c). These results indicate a weaker adsorption of $^*H$ at the surface of CoN_4-pyrr, which is beneficial for the rapid production of $^*H$ that can critically enhance the NRA kinetics. Besides, charge density difference analysis revealed that the electron transfer quantity from $^*H$ on the CoN_4-pyrr reached 0.48 e, compared to 0.42 e on the CoN_4-pyri, verifying its lower energy barrier for the $^*H$ transfer (Figure 4d; Figure S35, Supporting Information). The above results suggest that, compared to the CoN_4-pyri, the CoN_4-pyrr can exhibit a markedly lower activation energy and superior hydrogen adsorption characteristics in the

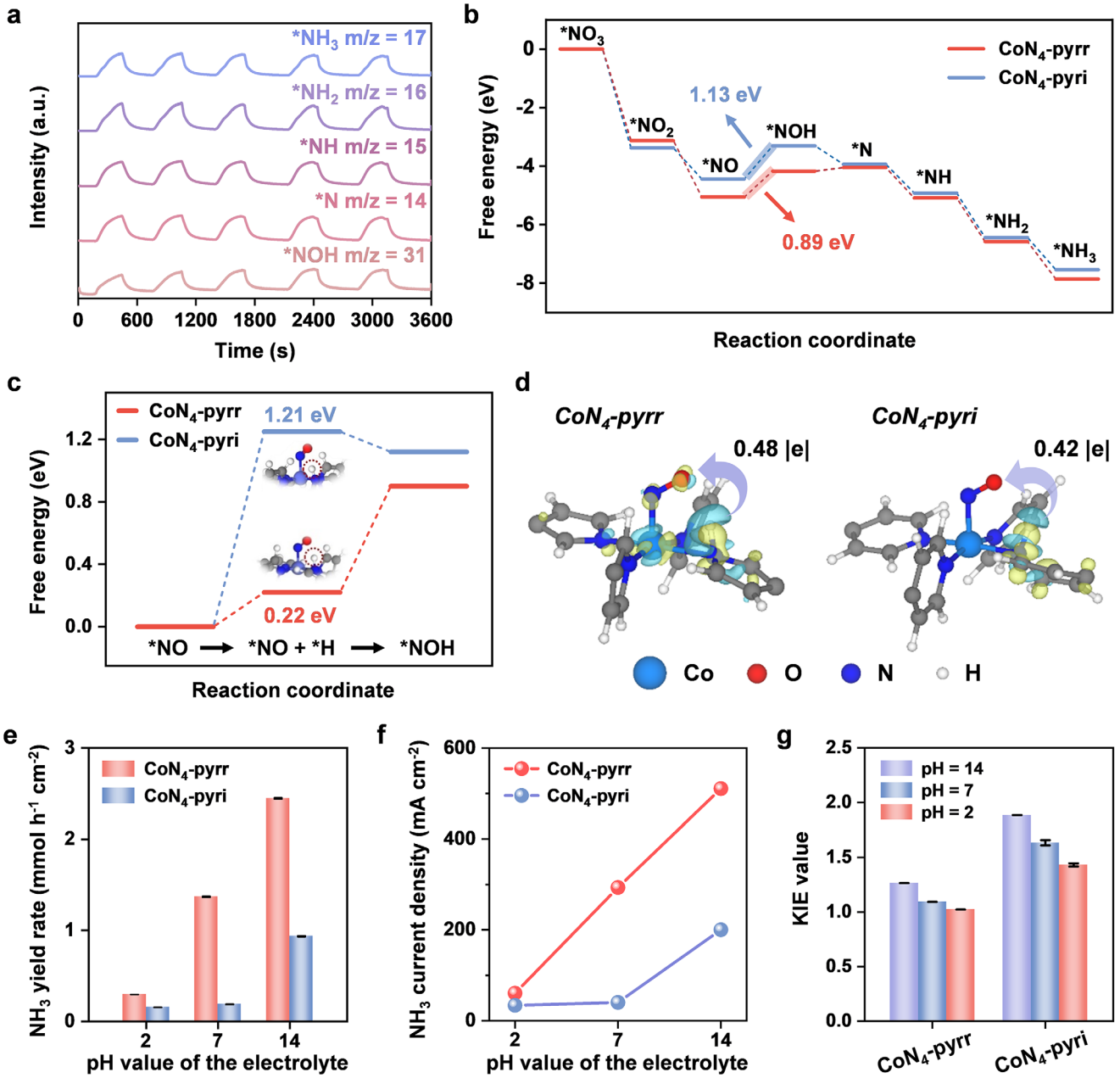

Figure 4. a) In situ DEMS measurements using the CoN_4-pyrr catalyst with detected signals of various NRA intermediates. b) Free energy diagram for the CoN_4-pyrr and CoN_4-pyri models for NRA catalysis. c) Comparison of the required energy barrier for hydrogenation of $^*NO$ into $^*NOH$ at the rate-determining step of NRA pathway, with $^*H$ transferred from the N atoms of pyrrole and pyridine ligands within CoN_4-pyrr and CoN_4-pyri, respectively. d) Charge density difference analysis for the $^*H$ transferring in CoN_4-pyri and CoN_4-pyrr (yellow: electron accumulation; cyan: electron depletion). Cyan, gray, red, blue and white balls represent Co, C, O, N, and H atoms, respectively. e,f) NH_3 yield rates and NH_3 current densities for CoN_4-pyrr and CoN_4-pyri electrodes measured under different pH conditions, respectively. g) Comparison of the KIE values for CoN_4-pyrr and CoN_4-pyri under different pH conditions. The KIE value is defined as the ratio of NH_3 current densities obtained with H_2O and D_2O as solvents.

critical hydrogenation step. Furthermore, pH-dependent electrochemical measurements were performed for the CoN_4-pyrr and CoN_4-pyri electrodes at −1.0 V (vs RHE) under different pH conditions (pH 2, 7, 14). As shown in Figure 4e,f, the NH_3 yield rate and NH_3 current density for CoN_4-pyrr both appreciably enhance as the pH value of electrolyte increases. In contrast, the NH_3 yield rate and NH_3 current density for the CoN_4-pyri both present less improvements. As observed, a significantly higher improvement in terms of activity and selectivity are achieved by the CoN_4-pyrr catalyst under high pH conditions, relative to the CoN_4-pyri. Besides, kinetic isotopic effect (KIE) experiments were conducted (Figure 4g; Figure S36, Supporting Information), which reveals lower KIE values for CoN_4-pyrr relative to those values for CoN_4-pyri, validating its faster hydrogenation kinetics along the

pathway of NRA. Under a higher pH condition, the kinetics of water dissociation would become more sluggish,[68,69] which would mitigate the competitive HER but also hinder the critical hydrogenation of *NO to from *NOH at the rate-determining step of NRA catalysis. In conjunction with the electrochemical measurements and DFT studies, these experimental results verify that, compared to the N atoms of pyridine ligand in the CoN_4-pyri, the N atoms of pyrrole ligand in the CoN_4-pyrr can achieve a faster transfer of *H to the Co active centers toward promoting the hydrogenation kinetics of *NO intermediates at the rate-determining step, accounting for its markedly higher NRA performance.

3. Conclusion

We demonstrate a facile and general approach to enhance the hydrogenation kinetics necessitated along the electrocatalytic nitrate reduction to ammonia (NRA) pathway by precisely regulating the coordination structures of single-atom metal sites in conjugated coordination polymers. Using cobalt (Co) as an example, two Co-single-atom enriched conjugated coordination polymer catalysts (CoN_4-pyrr and CoN_4-pyri) synthesized with pyrrole and pyridine ligands were studied. Our electrochemical measurements elucidate that the CoN_4-pyrr can achieve a superior NH_3 yield rate (1.93 mmol h^{-1} cm^{-2}) with a high NH_3 Faradaic efficiency (99.5%) under a current density of 380.3 mA cm^{-2}, which can substantially outperform its counterpart CoN_4-pyri for NRA electrocatalysis. Further, the theoretical calculations combined with the pH-dependent electrochemical measurements and kinetic isotope effect experiments indicate that, compared to the N atoms of pyridine ligand in CoN_4-pyri, the N atoms of pyrrole ligand in CoN_4-pyrr can markedly promote the transfer of *H and accelerate the hydrogenation kinetics of *NO intermediate on the Co active center at the rate-determining step toward NRA catalysis. In a broader context, such scenario utilizing a rapid *H-transferring strategy to achieve improvement of NRA activity and selectivity over conjugated coordination polymer catalysts with well-defined single-atom metal sites would prospectively provide a novel and effective methodology for the design of high-performance single-atom catalysts for widespread application across various catalytic reactions.

Supporting Information

Supporting Information is available from the Wiley Online Library or from the author.

Acknowledgements

S.Z., Y.L., Y.D., and H.W. contributed equally to this work. The authors are grateful for the financial support from the National Natural Science Foundation of China (No.52373211). The Computational studies benefit from the Marsden Fund Council from Government funding (No.21-UOA-237) and the Catalyst: Seeding General Grant (No.22-UOA-031-CGS). The DFT simulations were performed on the New Zealand eScience Infrastructure (NeSI) high-performance computing facility.

Conflict of Interest

The authors declare no conflict of interest.

Data Availability Statement

The data that support the findings of this study are available from the corresponding author upon reasonable request.

Keywords

ammonia electrosynthesis, conjugated coordination polymers, electrocatalytic nitrate reduction, hydrogenation kinetics

Received: November 29, 2024
Revised: April 3, 2025
Published online:

[1] B. Snyder, A. Turkiewicz, H. Furukawa, M. Paley, E. Velasquez, M. Dods, J. Long, *Nature* **2023**, *613*, 287.
[2] P. Xia, X. Pan, S. Jiang, J. Yu, B. He, P. Ismail, W. Bai, J. Yang, L. Yang, H. Zhang, M. Cheng, H. Li, Q. Zhang, C. Xiao, Y. Xie, *Adv. Mater.* **2022**, *34*, 2200563.
[3] H. Du, M. Chatti, R. Hodgetts, P. Cherepanov, C. Nguyen, K. Matuszek, D. MacFarlane, A. Simonov, *Nature* **2022**, *609*, 722.
[4] K. Chu, J. Qin, H. Zhu, M. Ras, C. Wang, L. Xiong, L. Zhang, N. Zhang, J. Martens, J. Hofkens, F. Lai, T. Liu, *Sci. China Mater.* **2022**, *65*, 2711.
[5] H. Zheng, Z. Ma, Y. Liu, Y. Zhang, J. Ye, E. Debroye, L. Zhang, T. Liu, Y. Xie, *Angew. Chem., Int. Ed.* **2024**, *63*, 202316097.
[6] S. Liu, T. Qian, M. Wang, H. Ji, X. Shen, C. Wang, C. Yan, *Nat. Catal.* **2021**, *4*, 322.
[7] H. Zheng, Y. Liu, Z. Ma, E. Debroye, J. Ye, L. Zhang, T. Liu, *ACS Nano* **2024**, *18*, 17642.
[8] Y. Cui, C. Sun, G. Ding, M. Zhao, X. Ge, W. Zhang, Y. Zhu, Z. Wang, Q. Jiang, *Sci. China Mater.* **2023**, *66*, 4387.
[9] W. Chen, X. Yang, T. Huang, Y. Li, X. Ren, S. Ye, Q. Zhang, J. Liu, *Compos. Commun.* **2023**, *43*, 101715.
[10] F. Chen, Z. Wu, S. Gupta, D. Rivera, S. Lambeets, S. Pecaut, J. Kim, P. Zhu, Y. Finfrock, D. Meira, G. King, G. Gao, W. Xu, D. Cullen, H. Zhou, Y. Han, D. Perea, C. Muhich, H. Wang, *Nat. Nanotechnol.* **2022**, *17*, 759.
[11] W. Zhong, Y. Chen, P. Chen, Q. Chen, C. Yang, N. Zhang, X. Liu, Z. Lin, *Angew. Chem., Int. Ed.* **2025**, 202503117.
[12] Y. Wang, A. Xu, Z. Wang, L. Huang, J. Li, F. Li, J. Wicks, M. Luo, D. Nam, C. Tan, Y. Ding, J. Wu, Y. Lum, C. Dinh, D. Sinton, G. Zheng, E. Sargent, *J. Am. Chem. Soc.* **2020**, *142*, 5702.
[13] F. Ni, H. Yang, Y. Wen, H. Bai, L. Zhang, C. Cui, S. Li, S. He, T. Cheng, B. Zhang, H. Peng, *Sci. China Mater.* **2020**, *63*, 2606.
[14] W. Chen, Z. Chen, Z. Huang, L. Zheng, X. Zhao, J. Hu, H. Cao, Y. Li, X. Ren, X. Ouyang, S. Ye, X. Yan, Q. Zhang, J. Liu, *Sci. China Mater.* **2023**, *66*, 3901.
[15] L. Zhang, S. Zhang, J. Bai, Y. Ding, J. Ye, Y. Song, E. Debroye, W. Fan, T. Liu, *Chem. Commun.* **2024**, *60*, 6821.
[16] Y. Li, S. Xiao, X. Li, C. Chang, M. Xie, J. Xu, Z. Yang, *Mat. Today Phys.* **2021**, *19*, 100431.
[17] L. Zhang, J. Bai, S. Zhang, Y. Liu, J. Ye, W. Fan, E. Debroye, T. Liu, *ACS Nano* **2024**, *18*, 22095.
[18] M. Wang, T. Hu, C. Wang, F. Du, H. Yang, W. Sun, C. Guo, C. M. Li, *Sci. China Mater.* **2023**, *66*, 2750.
[19] J. Bai, Y. Liu, Z. Ma, S. Zhang, G. Chao, H. Lin, E. Debroye, L. Zhang, T. Liu, *Sci. China Chem.* **2024**, *67*, 2063.
[20] Z. Wu, M. Karamad, X. Yong, Q. Huang, D. Cullen, P. Zhu, C. Xia, Q. Xiao, M. Shakouri, F. Chen, J. Kim, Y. Xia, K. Heck, Y. Hu, M. Wong, Q. Li, I. Gates, S. Siahrostami, H. Wang, *Nat. Commun.* **2021**, *12*, 2870.
[21] Z. Wu, J. Bai, F. Lai, H. Zheng, Y. Zhang, N. Zhang, C. Wang, Z. Wang, L. Zhang, T. Liu, *Sci. China Mater.* **2023**, *66*, 2680.

[22] M. A. Nazir, M. S. Javed, M. Islam, M. A. Assiri, A. M. Hassan, M. Jamshaid, T. Najam, S. S. A. Shah, A. Rehman, *Compos. Commun.* **2024**, *45*, 101783.
[23] Z. Li, S. Ji, Y. Liu, X. Cao, S. Tian, Y. Chen, Z. Niu, Y. Li, *Chem. Rev.* **2020**, *120*, 623.
[24] L. Zhang, Z. Ma, Z. Wu, Y. Liu, J. Bai, S. Zhang, E. Debroye, W. Fan, H. Lin, T. Liu, *Adv. Funct. Mater.* **2024**, *34*, 2404707.
[25] M. Wang, S. Li, Y. Gu, W. Xu, H. Wang, J. Sun, S. Chen, Z. Tie, J. Zuo, J. Ma, J. Su, Z. Jin, *J. Am. Chem. Soc.* **2024**, *146*, 20439.
[26] G. Chao, Y. Zhang, L. Zhang, W. Zong, N. Zhang, T. Xue, W. Fan, T. Liu, Y. Xie, *J. Mater. Chem. A* **2022**, *10*, 5930.
[27] Z. Shen, Y. Peng, X. Li, N. Li, H. Xu, W. Li, X. Guo, H. Pang, *Compos. Commun.* **2024**, *48*, 101933.
[28] Y. Liu, W. Qiu, P. Wang, R. Li, K. Liu, K. Omer, Z. Jin, P. Li, *Appl. Catal. B Environ.* **2024**, *340*, 123228.
[29] H. Q. Fu, M. Zhou, P. F. Liu, P. Liu, H. Yin, K. Z. Sun, H. G. Yang, M. Al-Mamun, P. Hu, H.-F. Wang, H. Zhao, *J. Am. Chem. Soc.* **2022**, *144*, 6028.
[30] H. Zheng, Y. Zhang, Y. Wang, Z. Wu, F. Lai, G. Chao, N. Zhang, L. Zhang, T. Liu, *Small* **2023**, *19*, 2205625.
[31] W. Cui, F. Gao, G. Na, X. Wang, Z. Li, Y. Yang, Z. Niu, Y. Qu, D. Wang, H. Pan, *Chem. Soc. Rev.* **2024**, *53*, 10253.
[32] S. Zheng, X. Yang, Z. Shi, H. Ding, F. Pan, J. Li, *J. Am. Chem. Soc.* **2024**, *146*, 26965.
[33] L. Sun, C. Dai, T. Wang, X. Jin, Z. Xu, X. Wang, *Angew. Chem., Int. Ed.* **2024**, *63*, 202320027.
[34] Y. Xiong, Y. Wang, J. Zhou, F. Liu, F. Hao, Z. Fan, *Adv. Mater.* **2024**, *36*, 2304021.
[35] S. Chen, X. Li, C. Kao, T. Luo, K. Chen, J. Fu, C. Ma, H. Li, M. Li, T. Chan, M. Liu, *Angew. Chem., Int. Ed.* **2022**, *61*, 202206233.
[36] H. Zhong, M. Wang, G. Chen, R. Dong, X. Feng, *ACS Nano* **2022**, *16*, 1759.
[37] K. Fan, C. Zhang, Y. Chen, Y. Wu, C. Wang, *Chem* **2021**, *7*, 1224.
[38] P. Kumar, K. Kannimuthu, A. Zeraati, S. Roy, X. Wang, X. Wang, S. Samanta, K. Miller, M. Molina, D. Trivedi, J. Abed, M. C. Mata, H. Al-Mahayni, J. Baltrusaitis, G. Shimizu, Y. Wu, A. Seifitokaldani, E. Sargent, P. Ajayan, J. Hu, M. Kibria, *J. Am. Chem. Soc.* **2023**, *145*, 8052.
[39] X. Liu, Y. Zhou, M. Tian, L. Zhang, Z. Liu, W. Cai, Z. Long, B. Liang, W. Yang, Q. Li, K. Bi, Z. Zhang, *Compos. Commun.* **2024**, *49*, 101963.
[40] J. Ni, J. Yan, F. Li, H. Qi, Q. Xu, C. Su, L. Sun, H. Sun, J. Ding, B. Liu, *Adv. Energy Mater.* **2024**, *14*, 2400065.
[41] S. Zhang, L. Yang, T. Yang, Y. Song, M. Jia, J. Yang, Y. Liu, X. Zhou, J. Tang, *Compos. Commun.* **2023**, *44*, 101757.
[42] M. Liu, M. Liu, W. Chen, F. Li, S. Cai, S. Lin, X. Chen, Z. Cai, *Angew. Chem., Int. Ed.* **2025**, *64*, 202421755.
[43] N. Zhang, T. Zhou, M. Chen, H. Feng, R. Yuan, C. Zhong, W. Yan, Y. Tian, X. Wu, W. Chu, C. Wu, Y. Xie, *Energy Environ. Sci.* **2020**, *13*, 111.
[44] Y. Zhang, H. Zheng, K. Zhou, J. Ye, K. Chu, Z. Zhou, L. Zhang, T. Liu, *Adv. Mater.* **2023**, *35*, 2209855.
[45] J. Cai, Y. Wei, A. Cao, J. Huang, Z. Jiang, S. Lu, S. Zang, *Appl. Catal. B: Environ.* **2022**, *316*, 121683.
[46] W. Zhang, H. Dong, L. Zhou, H. Xu, H. Wang, X. Yan, Y. Jiang, J. Zhang, Z. Gu, *Appl. Catal. B: Environ.* **2022**, *317*, 121750.
[47] J. Zhao, X. Ren, X. Liu, X. Kuang, H. Wang, C. Zhang, Q. Wei, D. Wu, *Chem. Eng. J.* **2023**, *452*, 139533.
[48] Z. Wang, S. Liu, X. Zhao, M. Wang, L. Zhang, T. Qian, J. Xiong, C. Yang, C. Yan, *ACS Mater. Lett.* **2023**, *5*, 1018.
[49] Z. Xi, J. Wang, B. Liu, X. Xu, P. Jing, R. Gao, J. Zhang, *J. Energy Chem.* **2023**, *83*, 32.
[50] E. Murphy, Y. Liu, I. Matanovic, S. Guo, P. Tieu, Y. Huang, A. Ly, S. Das, I. Zenyuk, X. Pan, E. Spoerke, P. Atanassov, *ACS Catal.* **2022**, *12*, 6651.
[51] P. Li, Z. Jin, Z. Fang, G. Yu, *Energy Environ. Sci.* **2021**, *14*, 3522.
[52] J. Yang, H. Qi, A. Li, X. Liu, X. Yang, S. Zhang, Q. Zhao, Q. Jiang, Y. Su, L. Zhang, J. Li, Z. Tian, W. Liu, A. Wang, T. Zhang, *J. Am. Chem. Soc.* **2022**, *144*, 12062.
[53] X. Cheng, J. He, H. Ji, H. Zhang, Q. Cao, W. Sun, C. Yan, J. Lu, *Adv. Mater.* **2022**, *34*, 2205767.
[54] J. Li, Y. Zhang, C. Liu, L. Zheng, E. Petit, K. Qi, Y. Zhang, H. Wu, W. Wang, A. Tiberj, X. Wang, M. Chhowalla, L. Lajaunie, R. Yu, D. Voiry, *Adv. Funct. Mater.* **2022**, *32*, 2108316.
[55] Y. Zhang, X. Chen, W. Wang, L. Yin, J. Crittenden, *Appl. Catal. B: Environ.* **2022**, *310*, 121346.
[56] Y. Xue, Q. Yu, Q. Ma, Y. Chen, C. Zhang, W. Teng, J. Fan, W. Zhang, *Environ. Sci. Technol.* **2022**, *56*, 14797.
[57] Y. Xu, M. Xie, H. Zhong, Y. Cao, *ACS Catal.* **2022**, *12*, 8698.
[58] X. Zhao, Z. Zhu, Y. He, H. Zhang, X. Zhou, W. Hu, M. Li, S. Zhang, Y. Dong, X. Hu, A. Kuklin, G. Baryshnikov, H. Ågren, T. Wågberg, G. Hu, *Chem. Eng. J.* **2022**, *433*, 133190.
[59] A. Kumar, J. Lee, M. Kim, B. Debnath, X. Liu, Y. Hwang, Y. Wang, X. Shao, A. Jadhav, Y. Liu, H. Tüysüz, H. Lee, *ACS Nano* **2022**, *16*, 15297.
[60] M. Xu, Q. Xie, D. Duan, Y. Zhang, Y. Zhou, H. Zhou, X. Li, Y. Wang, P. Gao, W. Ye, *ChemSusChem* **2022**, *15*, 202200231.
[61] L. Liu, T. Xiao, H. Fu, Z. Chen, X. Qu, S. Zheng, *Appl. Catal. B: Environ.* **2023**, *323*, 122181.
[62] J. Li, M. Li, N. An, S. Zhang, Q. Song, Y. Yang, J. Li, X. Liu, *Proc. Natl. Acad. Sci. USA* **2022**, *119*, 2123450119.
[63] H. Chen, C. Zhang, L. Sheng, M. Wang, W. Fu, S. Gao, Z. Zhang, S. Chen, R. Si, L. Wang, B. Yang, *J. Hazard. Mater.* **2022**, *434*, 128892.
[64] Y. Lv, J. Su, Y. Gu, B. Tian, J. Ma, J. Zuo, M. Ding, *JACS Au.* **2022**, *2*, 2765.
[65] J. Li, M. Li, N. An, S. Zhang, Q. Song, Y. Yang, X. Liu, *Proc. Natl. Acad. Sci. USA* **2021**, *118*, 2105628118.
[66] S. Han, H. Li, T. Li, F. Chen, R. Yang, Y. Yu, B. Zhang, *Nat. Catal.* **2023**, *6*, 402.
[67] R. Wang, S. Jia, L. Wu, L. Zhang, X. Song, X. Tan, C. Zheng, W. Li, X. Ma, Q. Qian, X. Kang, Q. Zhu, X. Sun, B. Han, *Angew. Chem., Int. Ed.* **2025**, *64*, 202425262.
[68] Y. Yao, C. Yin, W. He, Y. Zhou, C. Ma, Y. Liu, X. Li, C. Lu, *ACS Catal.* **2024**, *14*, 14912.
[69] W. Yu, H. Huang, Y. Qin, D. Zhang, Y. Zhang, K. Liu, Y. Zhang, J. Lai, L. Wang, *Adv. Energy Mater.* **2022**, *12*, 2200110.